Journal of Zhejiang University-SCIENCE A (Applied Physics & Engineering)
ISSN 1673-565X (Print); ISSN 1862-1775 (Online)
www.zju.edu.cn/jzus; www.springerlink.com
E-mail: jzus@zju.edu.cn

Experimental validation of sound quality simulation and optimization of a four-cylinder diesel engine

Jie MAO†, Zhi-yong HAO, Kang ZHENG, Guo-xi JING

(*Department of Energy Engineering, Zhejiang University, Hangzhou 310027, China*)

†E-mail: maojie1987@zju.edu.cn

Received Feb. 17, 2013; Revision accepted Apr. 7, 2013; Crosschecked Apr. 18, 2013

Abstract: A novel sound quality simulation approach was proposed to optimize the acoustic performance of a four-cylinder diesel engine. Finite element analysis, single-input and multiple-output technology, flexible multi-body dynamics, and boundary element codes were used to acquire the hexahedron-element model, experimental modal frequencies, vibration velocities, and structurally radiated noise of the block, respectively. The simulated modal frequencies and vibration velocities agreed well with the experimental data, which validated the finite-element block. The acoustic response showed that considerable acoustic power levels existed in 1500–1900 Hz and 2300–2800 Hz as the main frequency ranges to optimize the block acoustics. Then, the optimal block is determined in accordance with the novel approach, which reduces the overall value, high-frequency amplitudes, and peak values of acoustic power; thus, the loudness, sharpness, and roughness decline to make the sound quieter, lower-pitched, and smoother, respectively. Finally, the optimal block was cast and bench-tested. The results reveal that the sound quality of the optimal-block engine is substantially improved as numerically expected, which verifies the effectiveness of the research approach.

Key words: Diesel engine, Flexible multi-body dynamics, Sound quality simulation, Block optimization, Sound quality improvement

doi:10.1631/jzus.A1300055 **Document code:** A **CLC number:** TB532

1 Introduction

Vehicle noise perceived inside and outside the passenger cabin is one of the most significant factors in a consumer's judgment of the durability and quality of an automobile (Zuckerwar, 2010), which is driven by various excitations (Hussain *et al.*, 2007; Tsubokura *et al.*, 2010). Among the excitations, internal combustion engine noise is inevitable and must be considered due to its disturbance especially at higher revolving speeds (Hao *et al.*, 2007).

Diesel engine noise is constituted mainly of airborne noise and structure-borne noise (induced by combustion and mechanical motion) (Giakoumis, 2011). The airborne noise has been substantially decreased due to optimal design of intake air cleaners (Liu *et al.*, 2010) and exhaust mufflers (Liu *et al.*, 2012); its acoustic intensity is distinctly lower than that of the structure-borne noise. Hence, the current study aims to reduce the structure-borne noise and enhance the sound quality of a four-cylinder diesel engine. Regarding the structure-borne noise, it is known that the engine-order vibration influences the booming sound quality (Lee, 2008), which has been well controlled before this study by optimizing the damper at the free end and rubber mounting system of the engine. Consequently, the acoustic performance of the block is simulated and optimized to lower the structurally radiated noise of the diesel engine in the current study.

For a single structure uncoupled with a cavity (like an individual engine), the structurally radiated noise is dominated mainly by the global structural modes, while for a structure coupled with a cavity (like a vehicle with an engine and a cabin), the noise is related to the coupled modes (Theodossiades *et al.*,

© Zhejiang University and Springer-Verlag Berlin Heidelberg 2013

2004). The current work aims to enhance the sound quality of the diesel engine that is not coupled with the cabin cavity or other cavities, in other words, the structurally radiated noise is dominated mainly by the global structural modes, especially the modes of large components such as the block. Therefore, the global modes of the block are selected to analyze and optimize the radiated noise of the block and the engine.

Modal frequencies and excitation peak frequencies can be separated by improving structural stiffness, which is an effective approach to reducing the structurally radiated noise. Hambric (1995) investigated different approximation methods to optimize broad-band radiated noise problems, using a rib-stiffened cylindrical shell to prove the feasibility of different methodologies. Wang *et al.* (2012) reduced the structurally radiated noise of a diesel engine cylinder head cover by considering the static stiffness and multiple-objective function of Euclidean distance with finite element analysis (FEA) and boundary element analysis (BEA); however, the optimized cover was excited by the original set of boundary conditions, which affected the optimized structural response results. Lin *et al.* (2008) built a flexible multiple-body dynamic (FMBD) model of an internal combustion engine and predicted sound and vibration response of the block for noise reduction, with a modal reduction technique to reduce the given dynamic finite element model to one with fewer degrees of freedom while maintaining the dynamic characteristics of the system (Craig, 1981), whereas the engine sound quality (SQ) was not taken into account, which might lead to a dilemma that binaural hearing is unable to perceive acoustic power reduction.

In this study, FEA (Zienkiewicz *et al.*, 2005), FMBD (Boysal and Rahnejat, 1997; Perera *et al.*, 2010), and BEA (Brancati *et al.*, 2009; Brancati and Aliabadi, 2012) are integrated to analyze the modal attributes, dynamic responses, and radiated noise, respectively. Their performances are validated by corresponding experiments to ensure the accuracy of subsequent simulations. The novel sound quality simulation and optimization approach is proposed and also applied to block structure modification. Finally, the radiated sound powers from the engine and block surfaces are reduced; simultaneously, the loudness, sharpness, and roughness of the structurally radiated noise are decreased to make the sound quieter, lower-pitched, and smoother, respectively, which improves the sound quality of the diesel engine. The flow chart of the research approach is shown in Fig. 1.

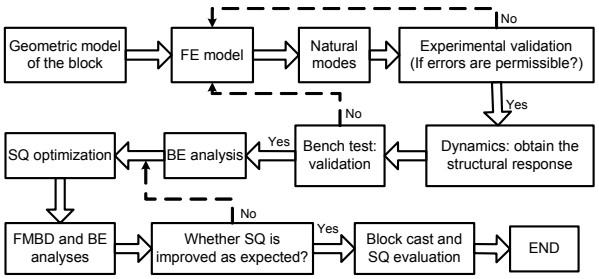

Fig. 1 Flow chart of the diesel engine sound quality simulation and optimization procedure

2 Sound quality simulation and optimization theory

Sound quality includes subjective and objective evaluations. Its engineering application dates back to the late 1980s. The subjective evaluation is based on experimental psychology, which is not discussed here in detail, while the objective evaluation establishes the relationship between psychological and physical parameters of sounds with the methods of neural network technology, time-frequency analysis, and objective parameter regression analysis (Lee, 2008).

Loudness, which directly affects other sound quality parameters such as sharpness and roughness, is the most fundamental parameter in sound quality objective evaluation theory (Menard *et al.*, 2008). Therefore, a simulation model of the structurally radiated sound loudness is proposed in this study, of which the result is utilized to calculate the sharpness and roughness. The structural optimization is implemented in accordance with the acoustic attributes of every sound quality parameter to reduce the loudness, sharpness, and roughness, in order to make the sound quieter, lower-pitched, and smoother, respectively, and improve the sound quality.

Considering the masking effect of a sound, critical bands are generally employed to describe the relationship between frequency selectivity and binaural hearing (Parizet and Koehl, 2012), and divide the audible frequency range (16–20 kHz) into 24 frequency bands (0–24 barks). However, in acoustic simulation issues, the specific frequency ranges are

selected as the computational domain for some specific targets, which can not only solve engineering problems, but also save considerable computational time. If the sound quality attributes of an acoustic event need to be analyzed like the radiated acoustic energy from the engine block surface concentrated in 1000–3000 Hz (Mao *et al*., 2013), very few critical bands are selected for analysis, which severely affects the result accuracy. Consequently, equivalent rectangular bandwidths (ERBs) (Sayles and Winter, 2010) take the place of critical bands in this study and divide the audible frequency range into approximately 40 bands, which improves the acoustic sensitivity of binaural and monaural hearing by taking the acoustic transfer function of the cochlea into consideration. The relationship between the equivalent rectangular bandwidth r and frequency f is defined in Eq. (1):

$$r = 21.366\lg(0.004368f + 1). \tag{1}$$

The excitation of a sound that reaches the cochlea is expressed as E. Accordingly, the excitation level is expressed as

$$L_E = 10\lg(E / E_0), \tag{2}$$

where E_0 is the reference excitation, representing the excitation at the output of the auditory filter centered at 1000 Hz produced by a 1000 Hz sinusoid presented at 0 dB sound pressure level in free field with frontal incidence.

In addition, the excitation at absolute threshold for monaural listening E_{TH} varies with frequency, but it remains approximately constant above 500 Hz (Mauermann *et al*., 2004), as listed in Table 1.

Table 1 Excitation level at absolute threshold for monaural listening in 1/3 octave band

f (Hz)	E_{TH} (dB)	f (Hz)	E_{TH} (dB)
50	28.18	200	8.08
63	23.90	250	6.30
80	19.20	315	5.30
100	15.68	400	4.50
125	12.67	500	3.63
160	10.09	>500	3.63

E_{TH} has been converted to decibel units (i.e., $10\lg E_{\mathrm{TH}}$)

The specific loudness is defined as the loudness in an equivalent rectangular bandwidth with the unit of sone/ERB, representing the loudness distribution characteristic in the frequency range of interest (Suzuki and Takeshima, 2004):

$$N' = \begin{cases} C\left(\dfrac{2E}{E+E_{\mathrm{TH}}}\right)^{1.5}[(GE+2E_{\mathrm{TH}})^{\alpha}-(2E_{\mathrm{TH}})^{\alpha}], \\ \qquad L_E < L_{E_{\mathrm{TH}}}, \\ C[(GE+2E_{\mathrm{TH}})^{\alpha}-(2E_{\mathrm{TH}})^{\alpha}],\ L_{E_{\mathrm{TH}}} < L_E < 100\ \mathrm{dB}, \\ C\left(\dfrac{E}{1.0707}\right)^{0.2},\ L_E > 100\ \mathrm{dB}, \end{cases} \tag{3}$$

where C is a constant with the value of 0.04687, and G is the low-level gain of the cochlear amplifier at a specific frequency, relative to the gain at 500 Hz and above (which is assumed to be constant). In general, if E_{TH} is a factor k higher than the value at 500 Hz and above, then G is equal to $1/k$. The value of α is the correction relative to the value of G, of which the relationship is listed in Table 2.

Table 2 Value of the parameter α as a function of parameter G

G (dB)	α	G (dB)	α
−25	0.267	−10	0.222
−20	0.250	−5	0.211
−15	0.237	0	0.200

G has been converted to decibel units (i.e., $10\lg G$)

Finally, the overall loudness N of a sound for monaural presentation is acquired by summing the values of the specific loudness N' across the ERB scale of interest, as defined in Eq. (4).

$$N = \int_{r_1}^{r_2} N'(r)\mathrm{d}r, \tag{4}$$

where r_1 and r_2 represent the lower and upper equivalent rectangular bandwidth rates of the computational domain, respectively.

As stated above, loudness is the decisive characteristic quantity for calculating sharpness and roughness.

Sharpness, in the unit of acum, is a measure of the high frequency content of a sound, which is expressed as

$$S=\frac{0.11}{N}\int_{r_1}^{r_2}L'(r)rg(r)\mathrm{d}r, \tag{5}$$

where S is sharpness, and $g(r)$ is a weighting function of different equivalent rectangular bandwidths, expressed as

$$g(r)=\begin{cases}1, & 0<r\le 25,\\ 0.066\mathrm{e}^{0.171r}, & 25<r\le 40.\end{cases} \tag{6}$$

Roughness, in the unit of asper, is one of auditory perception characteristics related to frequency modulation and amplitude modulation for sounds with frequency modulation at middle frequency around 70 Hz. In general, roughness R is calculated in accordance with modulation frequency f_{mod} and excitation level difference ΔL_E:

$$R=0.3f_{\mathrm{mod}}\int_{r_1}^{r_2}\Delta L_E(r)\mathrm{d}r\,. \tag{7}$$

3 Block mode analysis

The main parameters of the in-line four-cylinder diesel engine in this study are listed in Table 3.

Table 3 Main parameters of the diesel engine

Engine parameter	Value
Cylinder number	4
Cylinder diameter	93 mm
Compression ratio	18
Rated condition	75 kW, 3600 r/min
Maximal torque condition	250 N·m, 2000 r/min
Outline dimension	900 mm×545 mm×571 mm

The significance of analyzing the structural modal characteristics is embodied in two aspects:

1. Natural modes, as structural inherent attributes, are used to validate finite element model accuracy and ensure subsequent computation reliability by regulating the natural frequencies of numerical and mock-up models to permissible deviations (less than 10%).

2. The first several structural modes are dominated by global modes. While under excitations of these modal frequencies, global structural responses can be easily triggered or amplified, which will radiate structural noise.

According to finite element theory, in contrast with tetrahedron elements, hexahedron elements possess the advantages of faster solution speed, stronger distortion resistance, and higher computation accuracy (Owen and Saigal, 2001). Therefore, the hexahedron elements are employed to implement the block discretization process. The finite element model of the block is constituted of 182 548 elements (Fig. 2a). The block material is gray iron HT230, with the density, elastic modulus, and Poisson's ratio being 7280 kg/m^3, 120 000 MPa, and 0.265, respectively. Meanwhile, the boundary element model of the block is acquired with 6807 elements and 6280 nodes (Fig. 2b). Its element size is small and precise enough for the acoustic simulation in the frequency range of interest in Section 5.

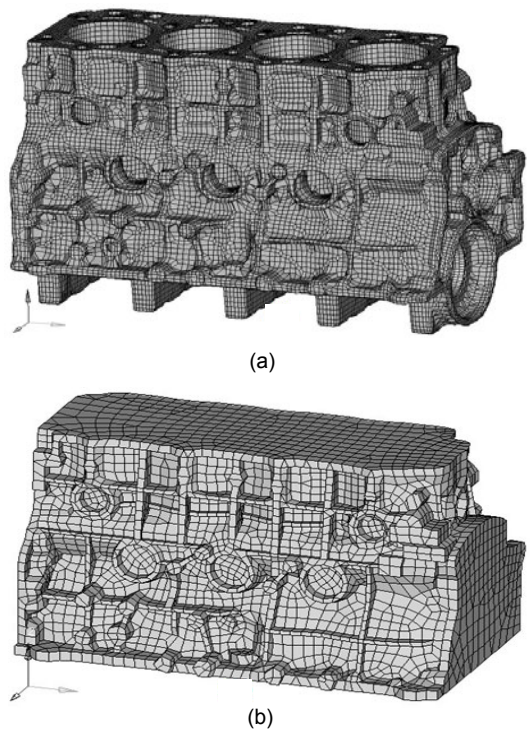

Fig. 2 The engine block model: (a) finite element model with hexahedron elements; (b) boundary element model

For evaluating the accuracy of the finite element model, the first 10 modal frequencies and vibration shapes from the simulation and experiment are obtained. The simulated modes are acquired by solving

eigenvalues with the Lanczos algorithm. The experimental modes are acquired by single-input and multiple-output technology using a perfectly flexible rope which has no influence on obtaining the natural modes. The measuring points on the block surface should be away from the structural vibration nodes where no responses can be acquired or the signal-to-noise ratio is low. The measuring points on the block surface and the first four simulated modal shapes are shown in Figs. 3 and 4, respectively. Table 4 lists the first 10 modal frequencies from the simulation and experiment.

As seen in Fig. 4 and Table 4, the first mode of the block at 625 Hz includes global torsional deformation; the second mode at 921 Hz involves bending deformation; the third mode at 1232 Hz consists of twisting and sheering deformation around the cylinder axis; and the fourth mode contains bending deformation which has vertical orientation with the second one.

In addition, Table 4 indicates the deviations between the first 10 simulated and experimental modal frequencies, ideally controlled below 5%, except the deviation of the fifth mode which is 5.7%. In general, the finite element model of the block possesses high accuracy in accordance with engineering permission (which is usually assumed as 10%) for subsequent computation reliability.

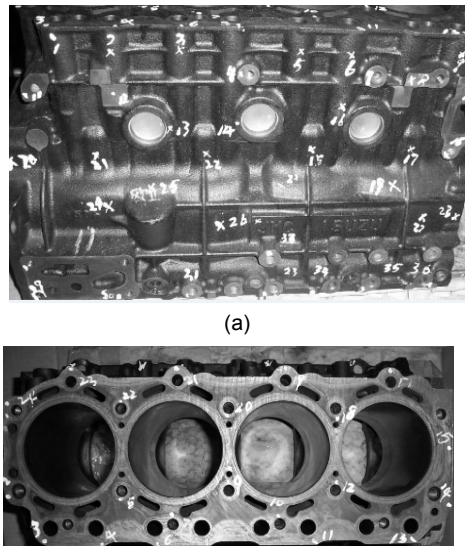

(a)

(b)

Fig. 3 Measuring points on the block for the natural modal test: (a) anti-thrust side of the block; (b) top surface of the block

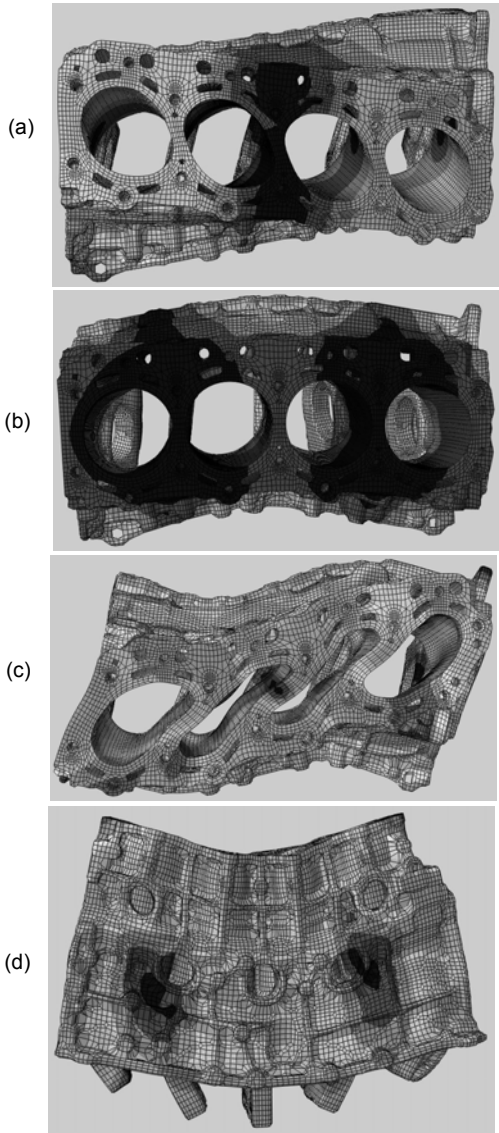

(a)

(b)

(c)

(d)

Fig. 4 The first (a), second (b), third (c), and fourth (d) natural modal shapes of the block

Table 4 Comparison of results from the simulation and experiment for the first 10 natural mode frequencies of the block

No.	Test frequency (Hz)	Calculated frequency (Hz)	Deviation (%)
1	628	625	−0.5
2	953	921	−3.4
3	1225	1232	0.6
4	1523	1471	−3.4
5	1649	1631	−1.1
6	1758	1658	−5.7
7	1833	1820	−0.7
8	1855	1859	0.2
9	1905	1948	2.3
10	2030	2014	−0.8

4 Dynamic prediction of the diesel engine

The finite element model of the diesel engine, including the block, cylinder head (cover), crankshaft, flywheel, oil pan, intake/exhaust manifolds, gearbox, and auxiliaries (brackets, electromotor, pumps, etc.), is constructed to calculate and evaluate the structural dynamic response. All these numerical models are composed of hexahedron elements and verified by modal experiment; their materials and element numbers are listed in Table 5. In Fig. 5a, the flywheel side of the engine is connected to the gearbox to make the numerical model as integral as the bench test, which can enhance the dynamic simulation accuracy.

Table 5 Basic parameters of the main finite-element components

Component	Material	Element number
Block	HT230	182 548
Crankshaft	Steel	89 172
Cylinder head	HT230	99 656
Cylinder head cover	Aluminum alloy	21 712
Flywheel	Steel	5532
Oil pan	Steel	5842
Intake manifold	Aluminum alloy	5771
Exhaust manifold	Steel	5516
Gearbox	Aluminum alloy	9201
Auxiliaries	Aluminum alloy/Steel	15 324

The rated condition (75 kW, 3600 r/min), under which the diesel engine possesses maximal output power, is selected to analyze the structural dynamic response of the block. For pledging simulation accuracy, the complete finite element model is constructed and cramped at the brackets (zero displacement at the bracket undersides) to form a three-point support; besides, correct connections between the components are required to ensure operating reliability. As shown in Fig. 5b, the damper at the free end of the engine (where no power outputs) is of great importance to attenuate torsional vibration of the crankshaft; moreover, different bearings are used to assemble corresponding components. For instance, the thrust bearings take the responsibility for keeping the crankshaft from shuttling in the axial direction.

In addition, accurate excitations imposed on the structures are significant factors for assuring precise dynamic results. The block is subjected to several excitations in the following ways: (1) the in-cylinder combustion induced gas pressures transmit to the block through cylinder head bolts, (2) the cylinder liner-piston contact induced lateral forces transmit through cylinder liners, and (3) the valve system motion induced impact forces directly apply to the block (which are valve seating forces) or transmit from bearings to the block (which are shaft rotation induced forces).

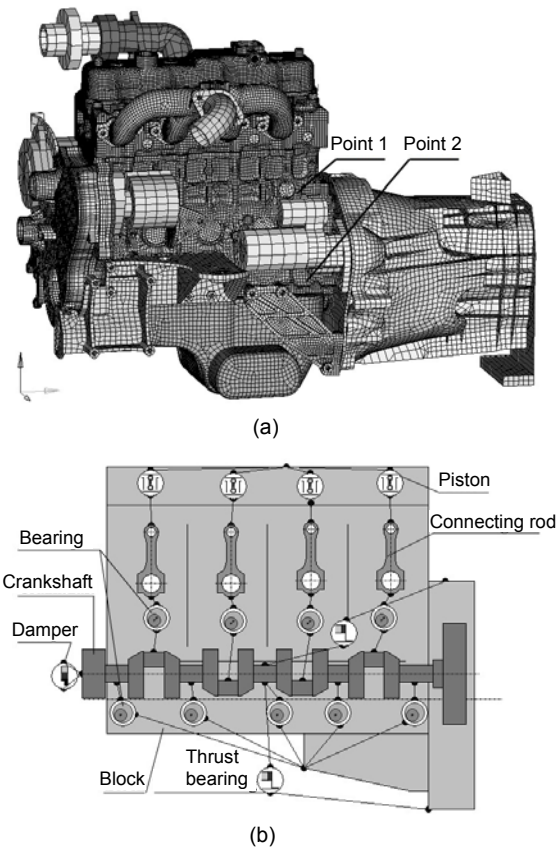

Fig. 5 Simulation models of the diesel engine: (a) finite element model; (b) dynamic model

Among the above-mentioned excitations, the gas pressures are experimentally measured by perforating appropriate keyholes at the top of the combustion chambers and arranging pressure transducers for data acquisition. As a typical in-line four-cylinder internal combustion engine, the power stroke sequence is in the cylinder order of 1-3-4-2 with the constant crank angle of 180° between contiguous power strokes (Fig. 6a) to ensure structural stationarity, just as the order for a V6 engine is of 1-5-3-6-2-4 (Fontanesi and Giacopini, 2013). Fig. 6b shows the gas force on the

piston top in the frequency domain. Generally speaking, the force has considerable amplitudes below 600 Hz, which mainly affects the engine vibration; however, its curve has peaks at higher frequencies, which primarily influences the structurally radiated noise.

The cylinder liner-piston contact induced force, also known as the lateral force, is composed of two aspects: (1) the quasi-static force induced by reciprocating inertial motion of the piston, relative to the basic parameters and gas pressures of the engine; (2) the secondary motion of the piston produced slap forces, which occurs at the moment of piston reversing and is caused by the factors of fluid lubrication, cylinder liner-piston clearance, and radial elastic deformation of the piston.

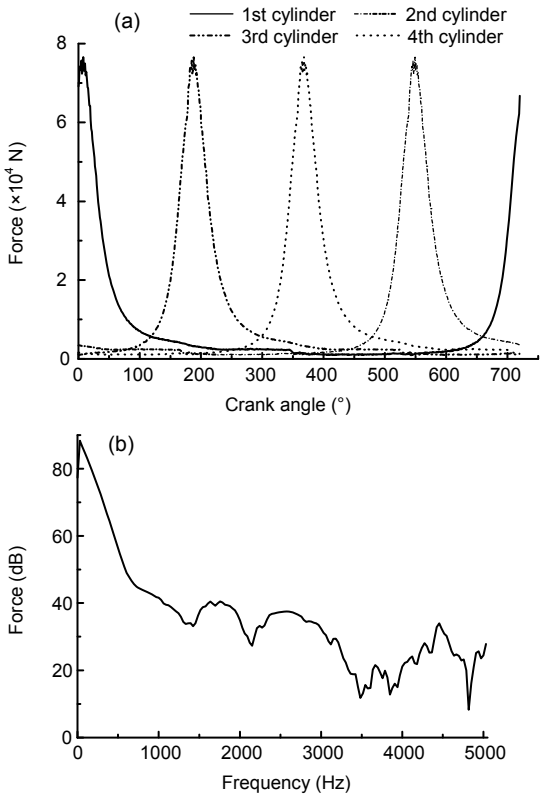

Fig. 6 In-cylinder combustion induced gas pressures under different crank angles (a) and frequencies (b) at the rated condition. Force has been converted to force level in decibel units (i.e., 20lg*F*)

Fig. 7a shows the lateral force in the third cylinder under different crank angles, which is calculated by piston dynamics (Wannatong *et al*., 2008), with the cylinder-piston clearance of 0.108 mm. It is indicated that the force can exceed 8000 N at the crank angle of 700° when the piston reverses.

Among the valve system motion induced excitations, the valve seating force, camshaft bearing force, and rocker bearing force mainly contribute to the engine noise. Fig. 7b presents the intake valve seating force of the third cylinder under different crank angles (the top dead center is marked). In the crank angle span of 0–246°, the third cylinder is proceeding an intake stroke during which the intake valve stays open with the force remaining at 0 N. When the crank angle reaches 246°, due to the end of the intake stroke, the valve closes and the maximal force occurs with the amplitude of 668 N. In addition, other excitations, without distinct characteristics, cannot be enumerated because of limited space.

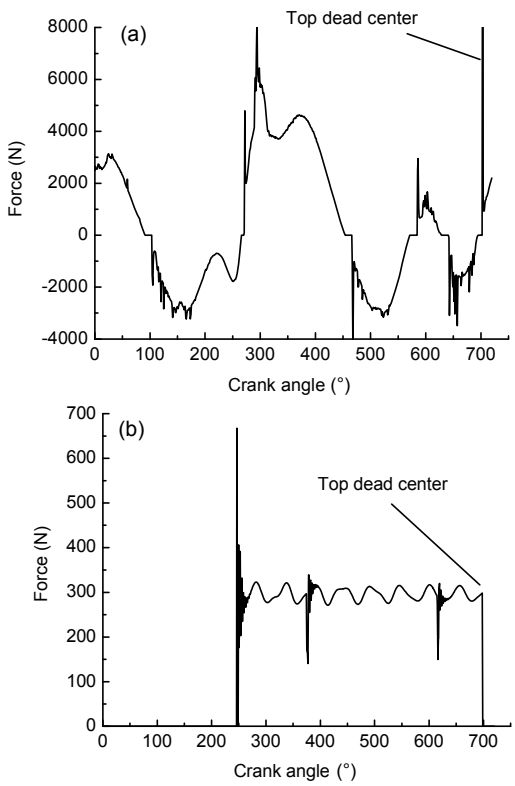

Fig. 7 Excitations of the third cylinder: (a) cylinder liner-piston contact inducted lateral force; (b) intake valve seating force

Finally, structural responses (displacements, velocities, or accelerations) from the block surface can be obtained after imposing the complete boundary conditions on the dynamic model of the diesel engine.

To validate dynamic simulation accuracy, a bench test of the diesel engine is conducted to measure the vibration responses from the block surface under the rated condition in a standard semi-anechoic room. The effective frequency response ranges of the signal sampling frequency and vibration transducers are 10.24 kHz and 0–10 kHz, respectively. During the bench test, the revolving speed of the diesel engine remains stable at 3600 r/min; besides, random measuring points, located at a certain distance from each other to pledge the high independence of the experimental data, are selected on the block surface (Fig. 5a). In this study, vibration velocity levels are adopted to evaluate the structural responses from the block surface, as expressed in Eq. (8).

$$L_v = 20\lg(v / v_0)\,, \tag{8}$$

where L_v is the velocity level, v is the vibration velocity of each measuring point, and v_0 is the reference velocity with value of 5×10^{-8} m/s.

Fig. 8 shows the vibration velocity level comparison results from the dynamic simulation and bench test of measuring points 1 and 2. As shown in Fig. 8a, the changing trend and amplitude of the vibration velocity level curve from the simulation agree well with those from the bench test of point 1, in spite of the reasonable disparity at some frequencies due to inevitable errors of the boundary conditions such as the added mass of the transducers and the necessary simplification of the system. For a complex system like an internal combustion engine, some excitations and boundary conditions have to be simplified to ensure the accuracy within minimal computational complexity. In Fig. 8b, the comparison results of point 2 are similar to those described for point 1. In general, the changing trend and amplitudes of the vibration velocity level of each measuring point in 0−3000 Hz from the dynamic simulation are consistent with that from the bench test, which proves that the numerical diesel engine model and simulation results are precise enough for engineering applications.

5 Sound quality simulation and optimization of the block

5.1 Sound quality simulation of the radiated noise from the block surface

The acoustic response from the block surface is obtained by the FEA-BEA methodology. Once normal components of the block surface vibration velocities are determined and validated as described above, acoustic powers in the frequency range of interest are computed via standard BEA codes (the sound propagation medium is air). Then, in accordance with the sound quality research procedure in Fig. 1, the structural noise can be reduced by block stiffness optimization to lower the loudness, sharpness, and roughness, which will make the sound quieter, lower-pitched, and smoother.

Commonly, the radiated acoustic energy of an internal combustion engine block is centered in 1000−3000 Hz. Therefore, in this study we analyze this frequency range so as to substantially cut down the computational time. Fig. 9 presents the radiated acoustic power levels from the block surface under different frequencies. Under the rated condition, the

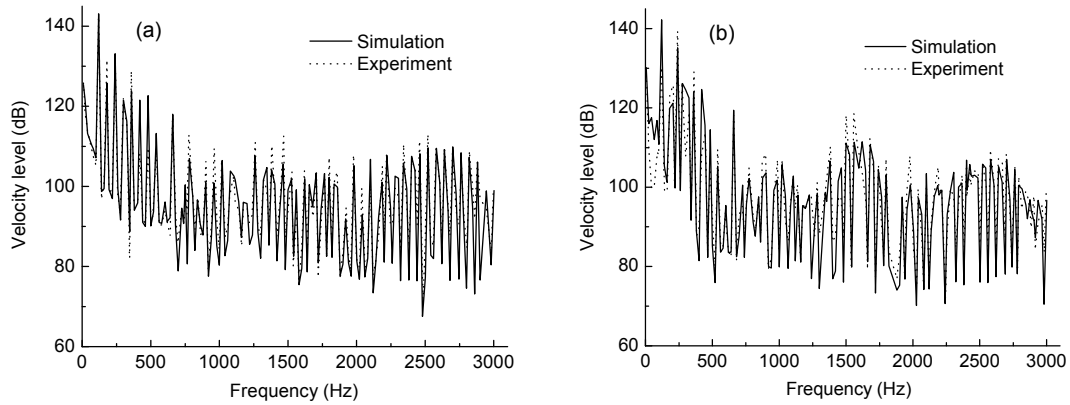

Fig. 8 Simulated and bench-tested vibration velocity level comparison results from the block surface at point 1 (a) and point 2 (b)

overall value of the structurally radiated acoustic power level curve of the original block is 86.2 dBA, and considerable peaks exist in 1500−1900 Hz and 2300−2800 Hz. For instance, the acoustic power levels at 1564 Hz and 2500 Hz are 71.5 dBA and 70.8 dBA, respectively. Besides, the loudness, sharpness, and roughness of the noise radiated from the original block are calculated according to Eqs. (4)−(7), with the values of 167.94 sone, 2.57 acum, and 0.72 asper, respectively.

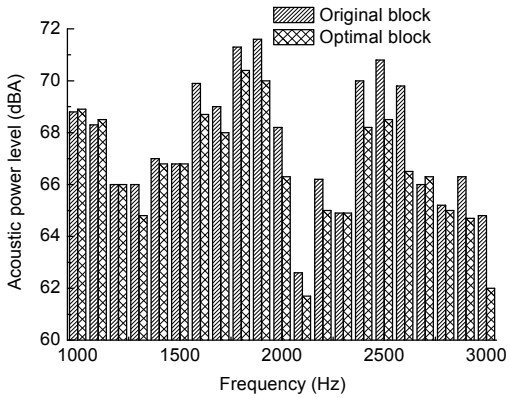

Fig. 9 Radiated acoustic power level from the block surface before and after optimization

As stated above, this study aims to reduce the radiated noise from the block surface and improve the sound quality of the diesel engine. Thus, optimal design for the original block is implemented and concentrated in the frequency ranges in which the considerable peaks occur. Hypothetically, the acoustic power overall value, high frequency peaks, and considerable amplitudes of the radiated noise from the modified block surface are decreased, which can reduce the loudness, sharpness, and roughness, respectively, and make the sound quieter, lower-pitched, and smoother.

5.2 Sound quality optimization of the radiated noise from the block surface

The block sound quality optimization should fulfill the following preconditions: (1) engine performances except noise, vibration, and harshness (NVH) attributes should not be negatively affected, (2) the new block can be cast and have no problems like structural connection, and (3) the sound quality parameters of the optimized radiated noise are lower than those of the original status.

The optimized schemes are implemented to enhance block stiffness (in order to separate the modal frequencies and the excitation peak frequencies, as explained in Section 1), reduce the radiated noise, and improve the sound quality. For each scheme, the computational procedure in Fig. 1 needs to be conducted again to obtain the structural response and sound quality of a new block.

Therefore, various schemes are proposed to achieve ideal frequency separation. Each new scheme is evaluated via observing whether the acoustic power levels of the block decline or not. If yes, this scheme can be utilized to build the next better one; if not, another different scheme should be proposed. After this optimization procedure, optimal design at the thrust side, anti-thrust side, and flywheel side of the block is determined, as shown in dark color in Fig. 10. The radiated acoustic power level of the optimal block is compared with that of the original one in Fig. 9. As a whole, the acoustic power levels in the frequency range of 1000−3000 Hz are decreased, especially at higher frequencies. For instance, the acoustic power levels at 1564 Hz and 2500 Hz of the optimal block are reduced by 1.8 dBA and 2.3 dBA, respectively, and the overall value is 0.8 dBA lower. Besides, the loudness, sharpness, and roughness of the optimal block are acquired with the values of 157.24 sone, 2.39 acum, and 0.66 asper, respectively, which substantially decline by 10.70 sone (6.37%), 0.18 acum (7.01%), and 0.06 asper (8.33%), respectively.

To sum up, the optimal scheme improves the acoustic attributes of the block in the following aspects:

1. The acoustic power level overall value is almost decreased by 1 dBA; hence, the radiated acoustic energy is 20% lower.

2. The loudness, sharpness, and roughness are substantially reduced by more than 6%, which will make the sound quieter, lower-pitched, and smoother, respectively.

3. The optimal block, served as the main excitation source for the radiated noise of other components (especially thin-walled parts), can decline NVH responses of the components, which will finally improve the engine sound quality.

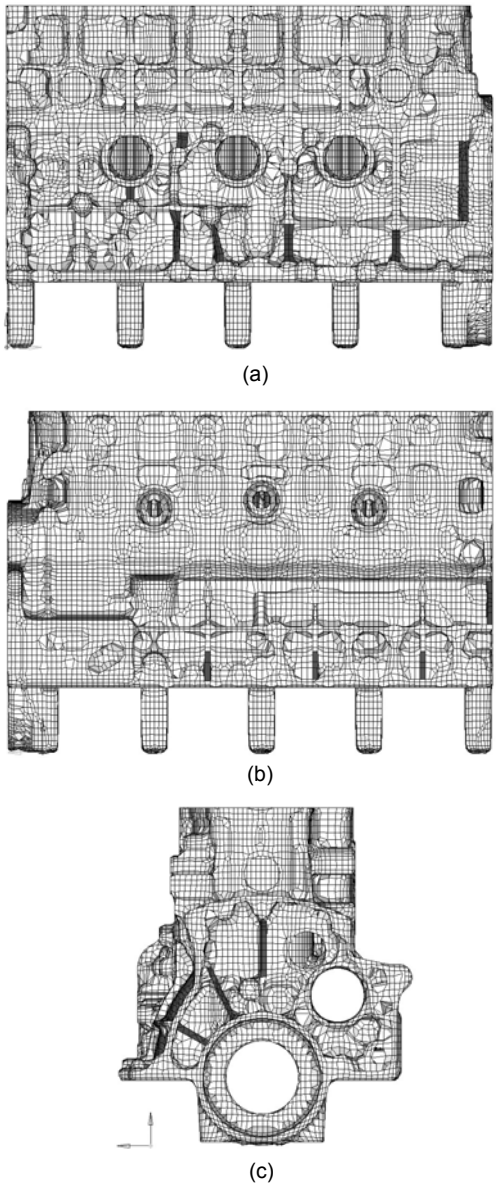

Fig. 10 Optimal scheme of the block (shown in dark color): (a) thrust side; (b) anti-thrust side; (c) flywheel side

6 Objective evaluation test of engine sound quality

The free end of an engine, which is of great importance for NVH study, has a significant influence on the acoustic performance of a bench test and an engine cabin. Besides, a sucking pump is placed at the end of the exhaust bellows to rapidly discharge the exhaust gas to outdoor space. Since the pumping noise will disturb the acoustic response at the thrust side and a uniform international standard for the engine sound quality objective evaluation has not been proposed so far, one measuring point that is one meter away from the free end center is chosen to measure the sound quality of the diesel engine.

Furthermore, a new block is cast in accordance with the optimal 3D model to validate effectiveness of the sound quality simulation and optimization theory. Thus, a bench test for sound quality evaluation is conducted after the replacement of the optimal block under the rated condition to obtain the sound quality parameters in the time domain and their overall values, as presented in Fig. 11 and Table 6, respectively.

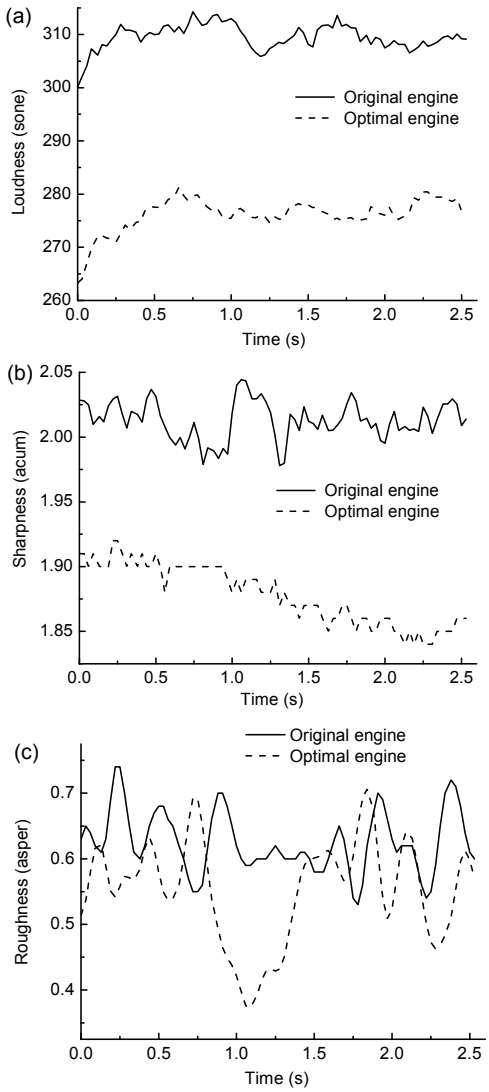

Fig. 11 Objective evaluation of the sound quality at the free end before and after optimal design: (a) loudness; (b) sharpness; (c) roughness

Table 6 Overall values of the sound quality evaluation at the free end before and after optimal design

Scheme	Loudness (sone)	Sharpness (acum)	Roughness (asper)
Original engine	309.52	2.01	0.63
Optimal engine	276.16	1.88	0.55
Deviation	10.78%	6.47%	12.70%

Under the rated condition, the loudness, sharpness, and roughness of the optimized diesel engine are 33.36 sone (10.78%), 0.13 acum (6.47%), and 0.08 asper (12.70%) lower than those of the original one, respectively. Besides, five acoustic experts are employed to subjectively evaluate the sound quality at the free end under the same condition. The survey of the acoustic performance change before and after optimal design shows that the sound at the free end is thought to be quieter, lower-pitched, and smoother due to the decline of the loudness, roughness, and sharpness, respectively.

To sum up, the results verify the feasibility and effectiveness of the sound quality simulation approach in numerical and experimental ways, which reduces the structurally radiated noise and improves the sound quality of the diesel engine.

7 Conclusions

This study develops the sound quality simulation-optimization approach and improves the sound quality of the diesel engine, which is validated by experiment. The innovative points and conclusions are summarized as follows:

1. The novel sound quality simulation and optimization approach is proposed and applied to improve the sound quality of the four-cylinder diesel engine by block structure modification, which is the first known case in this field.

2. The structural response from the block surface is studied by flexible multiple-body dynamics and validated by the bench test, which succeeds in achieving similar changing tendencies to pledge the subsequent sound quality simulation accuracy.

3. The optimal block is cast after comparison of various optimized schemes. The bench tests of the sound quality evaluation before and after the optimization are conducted. We succeed in finding out that the sound quality is substantially improved as numerically expected.

4. In numerical and experimental ways, the loudness, sharpness, and roughness are reduced successfully, which makes the sound of the diesel engine sound quieter, lower-pitched, and smoother, respectively.

Acknowledgements

The authors thank Jiangling Motors Co., Ltd. (JMC), China for sponsoring this study and casting the optimal block for the bench test.

References

Boysal, A., Rahnejat, H., 1997. Torsional vibration analysis of a multi-body single cylinder internal combustion engine model. *Applied Mathematical Modelling*, **21**(8):481-493. [doi:10.1016/S0307-904X(97)00032-2]

Brancati, A., Aliabadi, M.H., 2012. Boundary element simulations for local active noise control using an extended volume. *Engineering Analysis with Boundary Elements*, **36**(2):190-202. [doi:10.1016/j.enganabound.2011.06.008]

Brancati, A., Aliabadi, M.H., Benedetti, I., 2009. Hierarchical adaptive cross approximation GMRES technique for solution of acoustic problems using the boundary element method. *Computer Modeling in Engineering and Sciences*, **43**(2):149-172.

Craig, R.R., 1981. Structural Dynamics: an Introduction to Computer Methods. John Wiley & Sons, New Jersey, p.5-10.

Fontanesi, S., Giacopini, M., 2013. Multiphase CFD-CHT optimization of the cooling jacket and FEM analysis of the engine head of a V6 diesel engine. *Applied Thermal Engineering*, **52**(2):293-303. [doi:10.1016/j.applthermaleng.2012.12.005]

Giakoumis, E.G., 2011. Experimental study of combustion noise radiation during transient turbocharged diesel engine operation. *Energy*, **36**(8):4983-4995. [doi:10.1016/j.energy.2011.05.043]

Hambric, S.A., 1995. Approximation techniques for broadband acoustic radiated noise design optimization problems. *Journal of Vibration and Acoustics*, **117**(1):136-144. [doi:10.1115/1.2873857]

Hao, Z.Y., Jin, Y., Yang, C., 2007. Study of engine noise based on independent component analysis. *Journal of Zhejiang University-SCIENCE A*, **8**(5):772-777. [doi:10.1631/jzus.2007.A0772]

Hussain, K., Rahnejat, H., Hegazy, S., 2007. Transient vehicle handling analysis with aerodynamic interactions. *Journal of Multi-body Dynamics*, **221**(1):21-32. [doi:10.1243/1464419JMBD41]

Lee, S.K., 2008. Objective evaluation of interior sound quality in passenger cars during acceleration. *Journal of Sound and Vibration*, **310**(1-2):149-168. [doi:10.1016/j.jsv.2007.07.073]

Lin, Q., Hao, Z.Y., Jia, W.X., Liu, H., 2008. Prediction method of radiated noise by engine block. *Journal of Jiangsu University (Natural Science Edition)*, **29**(3):210-213, 217 (in Chinese).

Liu, C., Hao, Z.Y., Chen, X.R., 2010. Optimal design of acoustic performance for automotive air-cleaner. *Applied Acoustics*, **71**(5):431-438. [doi:10.1016/j.apacoust.2009.11.010]

Liu, L.Y., Hao, Z.Y., Liu, C., 2012. CFD analysis of a transfer matrix of exhaust muffler with mean flow and prediction of exhaust noise. *Journal of Zhejiang University-SCIENCE A (Applied Physics & Engineering)*, **13**(9):709-716. [doi:10.1631/jzus. A1200155]

Mao, J., Hao, Z.Y., Jing, G.X., Zheng, X., Liu, C., 2013. Sound quality improvement for a four-cylinder diesel engine by the block structure optimization. *Applied Acoustics*, **74**(1):150-159. [doi:10.1016/j.apacoust.2012.07.005]

Mauermann, M., Long, G.R., Kollmeier, B., 2004. Fine structure of hearing threshold and loudness perception. *Journal of the Acoustical Society of America*, **116**(2):1066-1080. [doi:10.1121/1.1760106]

Menard, M., Gallego, S., Berger-Vachon, C., Collet, L., Thai-Van, H., 2008. Relationship between loudness growth function and auditory steady-state response in normal-hearing subjects. *Hearing Research*, **235**(1-2):105-113. [doi:10.1016/j.heares.2007.10.007]

Owen, S.J., Saigal, S., 2001. Formation of pyramid elements for hexahedra to tetrahedral transitions. *Computer Methods in Applied Mechanics and Engineering*, **190**(34):4505-4518. [doi:10.1016/S0045-7825(00)00330-3]

Parizet, E., Koehl, V., 2012. Application of free sorting tasks to sound quality experiments. *Applied Acoustics*, **73**(1):61-65. [doi:10.1016/j.apacoust.2011.07.007]

Perera, M.S.M., Theodossiades, S., Rahnejat, H., 2010. Elasto-multi-body dynamics of internal combustion engines with tribological conjunctions. *Journal of Multi-body Dynamics*, **224**(3):261-277. [doi:10.1243/14644193JMBD242]

Sayles, M., Winter, I.M., 2010. Equivalent-rectangular bandwidth of single units in the anaesthetized guinea-pig ventral cochlear nucleus. *Hearing Research*, **262**(1-2):26-33. [doi:10.1016/j.heares.2010.01.015]

Suzuki, Y., Takeshima, H., 2004. Equal-loudness-level contours for pure tones. *Journal of the Acoustical Society of America*, **116**(2):918-933. [doi:10.1121/1.1763601]

Theodossiades, S., Gnanakumarr, M., Rahnejat, H., Menday, M., 2004. Mode identification in impact-induced high-frequency vehicular driveline vibrations using an elasto-multi-body dynamics approach. *Journal of Multi-body Dynamics*, **218**(2):81-94. [doi:10.1243/146441904323074549]

Tsubokura, M., Nakashima, T., Kitayama, M., Ikawa, Y., Doh, D.H., Kobayashi, T., 2010. Large eddy simulation on the unsteady aerodynamic response of a road vehicle in transient crosswinds. *International Journal of Heat and Fluid Flow*, **31**(6):1075-1086. [doi:10.1016/j.ijheatfluidflow.2010.05.008]

Wang, L.S., Hao, Z.Y., Jing, G.X., 2012. Low noise design of cylinder head cover based on multi-objective topography optimization. *Journal of Southwest Jiaotong University*, **47**(6):1064-1068 (in Chinese).

Wannatong, K., Chanchaona, S., Sanitjai, S., 2008. Simulation algorithm for piston ring dynamics. *Simulation Modelling Practice and Theory*, **16**(1):127-146. [doi:10.1016/j.simpat.2007.11.004]

Zienkiewicz, O.C., Taylor, R.L., Zhu, J.Z., 2005. The Finite Element Method: Its Basis and Fundamentals. Butterworth Heinemann, Boston, p.1-18.

Zuckerwar, A.J., 2010. Theory of compact nonporous windscreens for infrasonic measurements. *Journal of the Acoustical Society of America*, **127**(6):3327-3334. [doi:10.1121/1.3409402]